BMC Medical Imaging

RESEARCH

Open Access

Deep learning models based on multiparametric magnetic resonance imaging and clinical parameters for identifying synchronous liver metastases from rectal cancer

Jing Sun[1], Pu-Yeh Wu[2], Fangmin Shen[1], Xingfa Chen[1], Jieqiong She[3], Mingcong Luo[4], Feifei Feng[1] and Dechun Zheng[1*]

Abstract

Objectives To establish and validate deep learning (DL) models based on pre-treatment multiparametric magnetic resonance imaging (MRI) images of primary rectal cancer and basic clinical data for the prediction of synchronous liver metastases (SLM) in patients with Rectal cancer (RC).

Methods In this retrospective study, 176 and 31 patients with RC who underwent multiparametric MRI from two centers were enrolled in the primary and external validation cohorts, respectively. Clinical factors, including sex, primary tumor site, CEA level, and CA199 level were assessed. A clinical feature (CF) model was first developed by multivariate logistic regression, then two residual network DL models were constructed based on multiparametric MRI of primary cancer with or without CF incorporation. Finally, the SLM prediction models were validated by 5-fold cross-validation and external validation. The performance of the models was evaluated by decision curve analysis (DCA) and receiver operating characteristic (ROC) analysis.

Results Among three SLM prediction models, the Combined DL model integrating primary tumor MRI and basic clinical data achieved the best performance (AUC = 0.887 in primary study cohort; AUC = 0.876 in the external validation cohort). In the primary study cohort, the CF model, MRI DL model, and Combined DL model achieved AUCs of 0.816 (95% CI: 0.750, 0.881), 0.788 (95% CI: 0.720, 0.857), and 0.887 (95% CI: 0.834, 0.940) respectively. In the external validation cohort, the CF model, DL model without CF, and DL model with CF achieved AUCs of 0.824 (95% CI: 0.664, 0.984), 0.662 (95% CI: 0.461, 0.863), and 0.876 (95% CI: 0.728, 1.000), respectively.

Conclusion The combined DL model demonstrates promising potential to predict SLM in patients with RC, thereby making individualized imaging test strategies.

*Correspondence:
Dechun Zheng
dechun.zheng@139.com

Full list of author information is available at the end of the article

Clinical relevance statement Accurate synchronous liver metastasis (SLM) risk stratification is important for treatment planning and prognosis improvement. The proposed DL signature may be employed to better understand an individual patient's SLM risk, aiding in treatment planning and selection of further imaging examinations to personalize clinical decisions.

Clinical trial number Not applicable.

Keywords Diagnostic model, Rectal cancer, Deep learning radiomics, Magnetic resonance imaging, Synchronous liver metastases

Introduction

Colorectal cancer is the second leading cause of cancer-related deaths worldwide, with rectal cancer (RC) accounting for approximately one-third of these deaths [1, 2]. When colorectal cancer is initially diagnosed, nearly 15–25% of patients are found to have synchronous liver metastases (SLM) [3]. SLM is a major concern in rectal cancer, as it significantly impacts treatment options and prognosis. Surgical intervention remains the primary and potentially curative treatment option for patients with liver metastases, however, only 25% of patients are eligible for surgery at the time of diagnosis [3, 4]. Therefore, early screening and accurate diagnosis of SLM at the preoperative examination is crucial for treatment planning and prognosis improvement for RC patients.

Currently, the diagnosis of SLM involves a range of laboratory tests, physical examinations, tissue biopsies, molecular genetic testing, or medical imaging such as CT, MRI, and PET-CT. Some studies have found that laboratory tests such as carcinoembryonic antigen (CEA) and carbohydrate antigen 19 – 9 (CA19-9) can complement imaging in diagnosing distant metastasis of RC [5]. While histopathological examination is regarded as the gold standard of diagnosis, biopsy and molecular genetic testing are expensive, invasive, and challenging for small lesions, and significant intra-tumor heterogeneity within the same primary specimen may affect the result [6, 7]. Medical imaging is widely used for SLM diagnosis. A meta-analysis reported that the sensitivity and specificity of CT for the diagnosis of liver metastases were 82.1% and 73.5%, respectively, due to its limited resolution [8]. Additionally, small lesions may be overlooked due to a similar degree of attenuation to the surrounding parenchyma [9]. PET-CT, despite its high specificity of 99% in diagnosing liver metastases, had insufficient sensitivity, high examination costs, and radiation exposure, which restricted its clinical application [10]. MRI offers higher soft tissue contrast, which is recommended as first-line approach for the preoperative clinical evaluation of SLM [11]. However, it also has limited sensitivity in detecting intrahepatic lesions smaller than 1 cm [12]. These traditional imaging methods primarily rely on qualitative features, making early and accurate diagnosis of small lesions with atypical signals or enhancement patterns challenging. Patients with atypical lesions may experience treatment delays while awaiting further confirmatory examination or may require risky invasive tests. Therefore, an accurate, rapid, noninvasive, and practical tool for SLM risk stratification is necessary.

Radiomics, utilizing high-throughput extraction of image features and machine learning algorithm, provides extensive information on the microstructure of the lesion [13]. Previous studies have developed prediction models based on features from relatively simple MR images, demonstrating promising prospects for MRI-based radiomics in predicting synchronous distant metastasis in patients with primary RC [14, 15]. However, these models have certain limitations. Furthermore, based on convolutional neural network, the deep learning (DL) technique can automatically learn crucial information from raw image data to perform tasks such as detection, classification, and segmentation [16]. Initial findings have demonstrated that DL achieves high accuracy in predicting response to chemotherapy, distant metastases, and prognosis in RC patients [17].

In this study, we aimed to utilize DL approaches to construct a classification model for the noninvasive prediction of SLM in patients with RC, solely using routinely acquired examination data.

Materials and methods

Institutional review board approval was obtained from two medical institutions, Clinical Oncology School of Fujian Medical University and Fujian Medical University Union Hospital (approval numbers: K2022-196-01 and 2023KY117). Given the retrospective nature of this study, the requirement for informed consent was waived.

Study cohorts: Primary study cohort

Consecutive patients who underwent rectal MRI examinations in our hospital between January 2014 and May 2020 were retrospectively collected and evaluated. The inclusion criteria were: (1) patients with histopathological confirmed primary rectal adenocarcinoma; (2) SLM confirmed by imaging examinations (CT, MRI, or ultrasonography) or pathology at the time of rectal cancer diagnosis; (3) no history of malignant neoplasm or other malignant neoplasms in combination. The exclusion

criteria were: (1) patients with metachronous distant metastases during one year of follow-up (to minimize misclassification of "non-SLM" cases with undetected micrometastases below imaging detection thresholds); (2) patients with mucinous adenocarcinoma or neuroendocrine carcinoma; (3) poor image quality, such as motion artifact, magnetic susceptibility artifacts and low SNR, which might lead to preclude accurate lesion interpretation; (4) incomplete clinical information.

Clinical characteristics were recorded, including age, sex, and primary tumor site. The levels of serum tumor markers, including carcinoembryonic antigen (CEA) and carbohydrate antigen 19 – 9 (CA199) levels, during the same period of rectal MRI were also recorded. Finally, 176 patients were included in the primary study cohort and were divided into non-SLM and SLM groups. Patients who were found to have metastatic lesions at diagnosis of primary rectal cancer were categorized into the SLM group. Liver-specific contrast-enhanced MRI was used as the preferred modality for assessing liver metastases. A multimodal imaging approach, combining ultrasound, CT, and MRI, was employed for comprehensive evaluation. All imaging data were reviewed by experienced radiologists, and discrepancies were resolved through multidisciplinary team discussions to ensure diagnostic accuracy. For atypical lesions, further confirmation was performed through follow-up imaging within one year or percutaneous biopsy. The non-SLM group was defined as patients with no metastases at primary staging and no evidence of metastases at 1 year of follow-up.

Study cohorts: External validation cohort

To further assess the validity and generalizability of the proposed DL model, we also collected external validation data from another institution. Consecutive patients who underwent rectal MRI examination between August 2017 and August 2020 were retrospectively evaluated using the same inclusion and exclusion criteria. Finally, 31 patients were included in the external validation cohort.

Image acquisition and segmentation

All enrolled patients underwent bowel preparation followed by rectal MRI examination before receiving treatment. MRI examinations were performed in the supine position on a 3.0T MRI scanner (Signa HDxt; GE Healthcare, Milwaukee, WI, USA) equipped with an eight-channel phased-array body coil. Axial T1-weighted imaging (T1WI), T2-weighted imaging (T2WI), diffusion-weighted imaging (DWI), and contrast-enhanced T1-weighted imaging (T1CE) were acquired. For the T1CE acquisition, a bolus of Gd-DTPA (gadopentetate dimeglumine, BeiLu Pharmaceutical, Beijing, China) at 0.1 mmol/kg was injected at a rate of 2 ml/s by a power injector. The detailed acquisition parameters are presented in Supplementary Material Table S1. Apparent diffusion coefficient (ADC) maps were calculated from DWI by mono-exponential fitting using Advantage Workstation 4.6 (GE Healthcare, Milwaukee, WI, USA). Tumor regions of interest (ROIs) were semi-automatically delineated on each consecutive slice of oblique axial high resolution T2WI using ITK-SNAP 3.8.0 software (www.itksnap.org). All ROIs were delineated by a junior radiologist (with 5 years of diagnostic experience) and reviewed by a senior radiologist (with 18 years of GI diagnostic experience). The ROIs were contoured along the margin of each tumor slice, avoiding air and necrotic areas of the tumor. Using ITK-SNAP's automatic expansion tool, this process was repeated for each slice to ensure thorough and accurate delineation of the entire tumor volume. Manual corrections were used to address ambiguities caused by adjacent tissues or artifacts.

Image preprocessing

All data from the primary study cohort were randomly divided into training and validation datasets in an 8:2 ratio. For image preprocessing, we first performed a rigid registration among multiparametric MRI images using SPM12 software (http://www.fil.ion.ucl.ac.uk/spm/). The resampling was carried out using linear interpolation to align the images. Images were then resampled into the same matrix size as that in T2WI (256×256) by cubic B-spline interpolation method. To account for variability in signal intensities, we applied z-score standardization to each MRI sequence. This normalization step ensured that the intensities across different sequences were standardized, facilitating better comparison and feature extraction. For the training dataset, if the number of tumor slices was >5, then 5 slices were chosen in the middle of the tumor. Subsequently, data were augmented by random cropping (according to the tumor center), random flipping (along the left-right axis), and random rotating ($\pm 10°$), resulting in a total of 12,200 2D patches (112×112) in the training dataset. Data from the external validation cohort were also preprocessed with the same procedure. All data processing was done using MATLAB 2018a (MathWorks, Natick, MA, USA).

SLM prediction model construction

A clinical feature (CF) model based on sex, primary tumor site, CEA, and CA199 was developed. Discriminative features between two groups were first selected by univariate logistic regression with a threshold of $P<0.1$. Subsequently, the CF model was constructed using multivariate logistic regression with a backward stepwise likelihood ratio selection method. For the DL model, a 2D ResNet was constructed based on the architecture of the residual network published previously [18] (Fig. 1). Specifically, input images consisted of 2D patches with

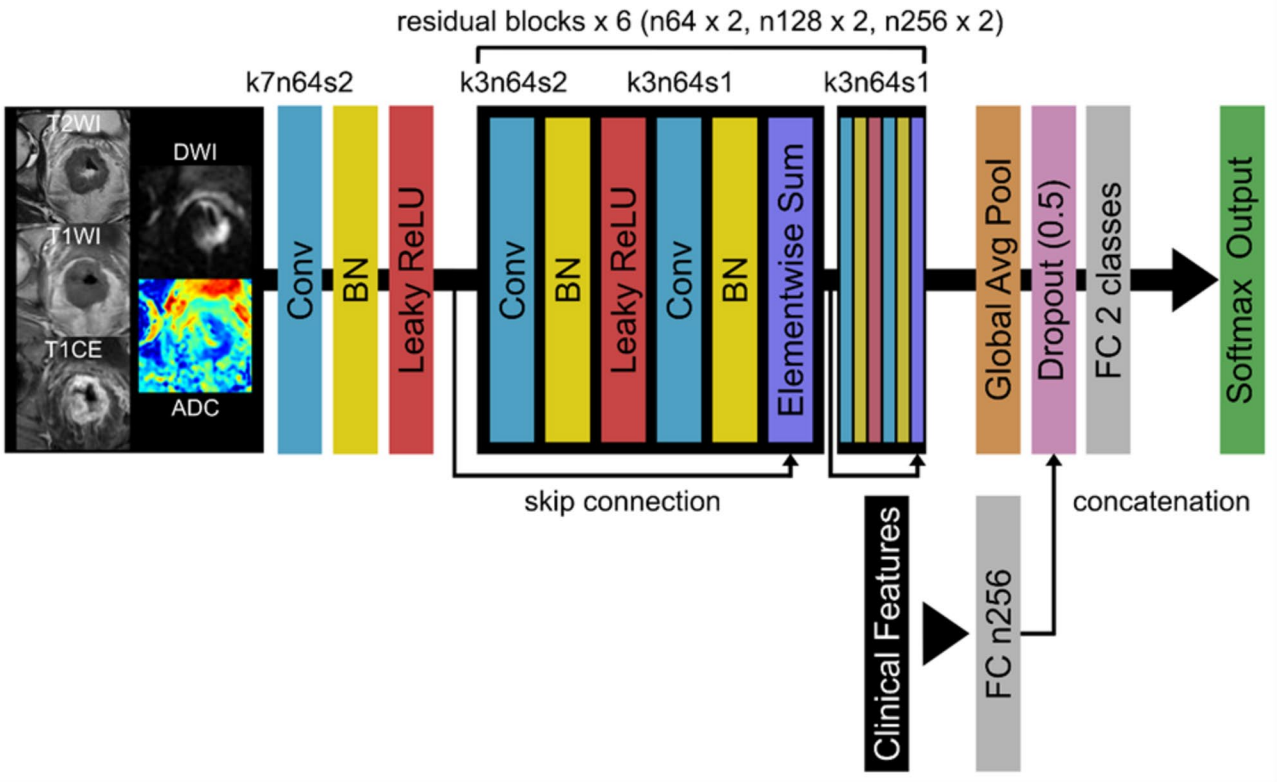

Fig. 1 Schematic diagram of the input data and DL (deep learning) framework

5 channels (T2WI, T1WI, T1CE, DWI, and ADC maps). Following 1 convolution layer with 7 × 7 filters and a stride of 2, there were 6 residual blocks consisted of 12 convolution layers with 3 × 3 filters and 6 skip connections. The leaky ReLU (alpha = 0.2) activation function was adopted. Clinical features were incorporated into the network using a fully-connected layer and concatenation before the classifier layer. The network ended with a global average pooling, a dropout layer, and a 2-way classifier with softmax activation function. For the optimization, we used Adam optimizer [19] with initial learning rate = 5×10^{-6} to minimize the cross-entropy loss with L1 and L2 regularization. The learning rate was exponentially decayed with a constant of 0.1, the batch size was set at 32, and the total number of epochs was set at 100. The network was trained using TensorFlow [20] with two NVIDIA Quadro GV100 GPUs. Two DL models were constructed with (Combined DL model) or without (MRI DL model) the CF incorporation. Finally, the SLM prediction model was validated by 5-fold cross-validation and external validation.

Statistical analysis

Statistical analysis of clinical characteristics was performed using SPSS 22.0 software (IBM Corp, Armonk, NY, USA). P values < 0.05 were considered statistically significant. Normally distributed quantitative variables were expressed as mean § standard deviations (SD). For the comparison of patient characteristics, categorical and continuous data were compared using Pearson's chi-square test (or Fisher's exact test) and Student's t-test (or Mann-Whitney U test), respectively. The performance of the model in predicting SLM was evaluated by receiver operating characteristic (ROC) analysis, and the area under the ROC curve (AUC) was recorded. AUCs of different models were compared by DeLong's test. Specific performance metrics, including accuracy (ACC), sensitivity (SEN), specificity (SPE), positive predictive value (PPV), and negative predictive value (NPV) at the median score threshold were also calculated. Decision curve analysis (DCA) was applied to validate the clinical value of the model. Univariate logistic regression was used to analyze the association between biological characteristics and DL scores.

Results

Clinical characteristics

A total of 176 patients (123 males and 53 females; age: 57.72 ± 10.21 years; age range: 28–85 years) were included in the primary study cohort. The median follow-up time was 33 months (range: 3–84 months). The external validation cohort comprised 31 patients (22 males and 9 females; age: 56.55 ± 16.78 years; age range: 24–83 years). 72 of 176 cases (40.9%) and 10 of 31 cases (32.3%) had

Table 1 Clinical characteristics of the primary cohort

Characteristic	Total	Non-SLM (*n* = 102)	SLM (*n* = 50)	*P* value
Sex, n (%)				0.058
Male	123 (69.9%)	67 (54.5%)	56 (45.5%)	
Female	53 (30.1%)	37 (69.8%)	16 (30.2%)	
Age, years	57.72 ± 10.21	57.12 ± 9.02	58.60 ± 11.72	0.368
Primary tumor site, cm	5.80 (3.15)	5.30 (2.60)	6.35 (5.00)	0.011
CEA level, n (%)				<0.001
Normal (< 5 ng/ml)	87 (49.4%)	66 (75.9%)	21(24.1%)	
Elevated (≥ 5 g/ml)	89 (50.6%)	38 (42.7%)	51 (57.3%)	
CA199 level, n (%)				<0.001
Normal (< 37 U/ml)	124 (70.5%)	95 (76.6%)	29 (23.4%)	
Elevated (≥ 37/ml)	52 (29.5%)	9 (17.3%)	43 (82.7%)	

Abbreviations: CA19-9, carbohydrate antigen 19 – 9; CEA, carcinoembryonic antigen

Quantitative data are reported as means ± standard deviations or medians with interquartile ranges

Table 2 Clinical characteristics of the external validation cohort

Characteristic	Total	Non-SLM (*n* = 21)	SLM (*n* = 10)	*P* value
Sex, n (%)				0.68
Male	22 (71.0%)	14 (63.6%)	8 (36.4%)	
Female	9 (29.0%)	7 (77.8%)	2 (22.2%)	
Age, years	56.55 ± 16.78	52.71 ± 17.45	64.60 ± 12.45	0.064
Primary tumor site, cm	5.2(4.0)	5.1 (3.7)	6.4 (4.8)	0.173
CEA level, n (%)				0.018
Normal (< 5 ng/ml)	17 (54.8%)	15 (88.2%)	2 (11.8%)	
Elevated (≥ 5 g/ml)	14 (45.2%)	6 (42.9%)	8 (57.1%)	
CA199 level, n (%)				0.001
Normal (< 37 U/ml)	26 (83.9%)	21 (80.8%)	5 (19.2%)	
Elevated (≥ 37 U/ml)	5 (16.1%)	0 (0%)	5 (100%)	

Abbreviations: CA19-9, carbohydrate antigen 19 – 9; CEA, carcinoembryonic antigen

Quantitative data are reported as means ± standard deviations or medians with interquartile ranges

SLM in the primary and external validation cohorts, respectively. The detailed clinicopathological characteristics of patients and comparison results are summarized in Tables 1 and 2.

The primary cohort showed a statistical difference in clinical characteristics (primary tumor site, CEA level, CA199 level) between SLM and non-SLM-negative groups (all $P < 0.05$), except age was detected between two groups. In the external validation cohort, we found the CEA level and CA199 level were different between two groups (both $P < 0.05$).

Diagnostic performance of the SLM prediction model

In the primary cohort, the CF model, MRI DL model, and Combined DL model achieved cross-validation AUCs of 0.816 (95% CI: 0.750, 0.881), 0.788 (95% CI: 0.720, 0.857), and 0.887 (95% CI: 0.834, 0.940), respectively. The AUC of Combined DL model was significantly higher than that of MRI DL model ($P = 0.010$), and was also higher than that of CF model but without significance ($P = 0.064$). For the CF model, the ACC, SEN, SPE, PPV, and NPV were 77.8% (137/176 patients), 61.1% (44/72 patients), 89.4% (93/104 patients), 80.0% (44/55 patients), and 76.9% (93/121 patients), respectively. For the MRI DL model, the ACC, SEN, SPE, PPV, and NPV were 75.6% (133/176 patients), 59.7% (43/72 patients), 86.5% (90/104 patients), 75.4% (43/57 patients), and 75.6% (90/119 patients), respectively. For the Combined DL model, the ACC, SEN, SPE, PPV, and NPV were 85.8% (151/176 patients), 80.6% (58/72 patients), 89.4% (93/104 patients), 84.1% (58/69 patients), and 86.9% (93/107 patients), respectively. Worth noting that if we focused on patients with liver metastasis smaller than 3 cm, we found a drop of SEN for the CF model from 61.1 to 51.0% (25/49 patients), while it remained constant for the MRI DL model from 59.7 to 59.2% (29/49 patients). The representative input images and the successful and unsuccessful predictions by the Combined DL model are presented in Fig. 2. ROC curves discriminating non-SLM and SLM groups from three models in the primary study cohort are shown in Fig. 3A.

Similarly, in the external validation cohort, the CF model, MRI DL model, and Combined DL model achieved external validation AUCs of 0.824 (95% CI: 0.664, 0.984), 0.662 (95% CI: 0.461, 0.863), and 0.876 (95% CI: 0.728, 1.000), respectively. For the CF model, the ACC, SEN, SPE, PPV, and NPV were 83.9% (26/31

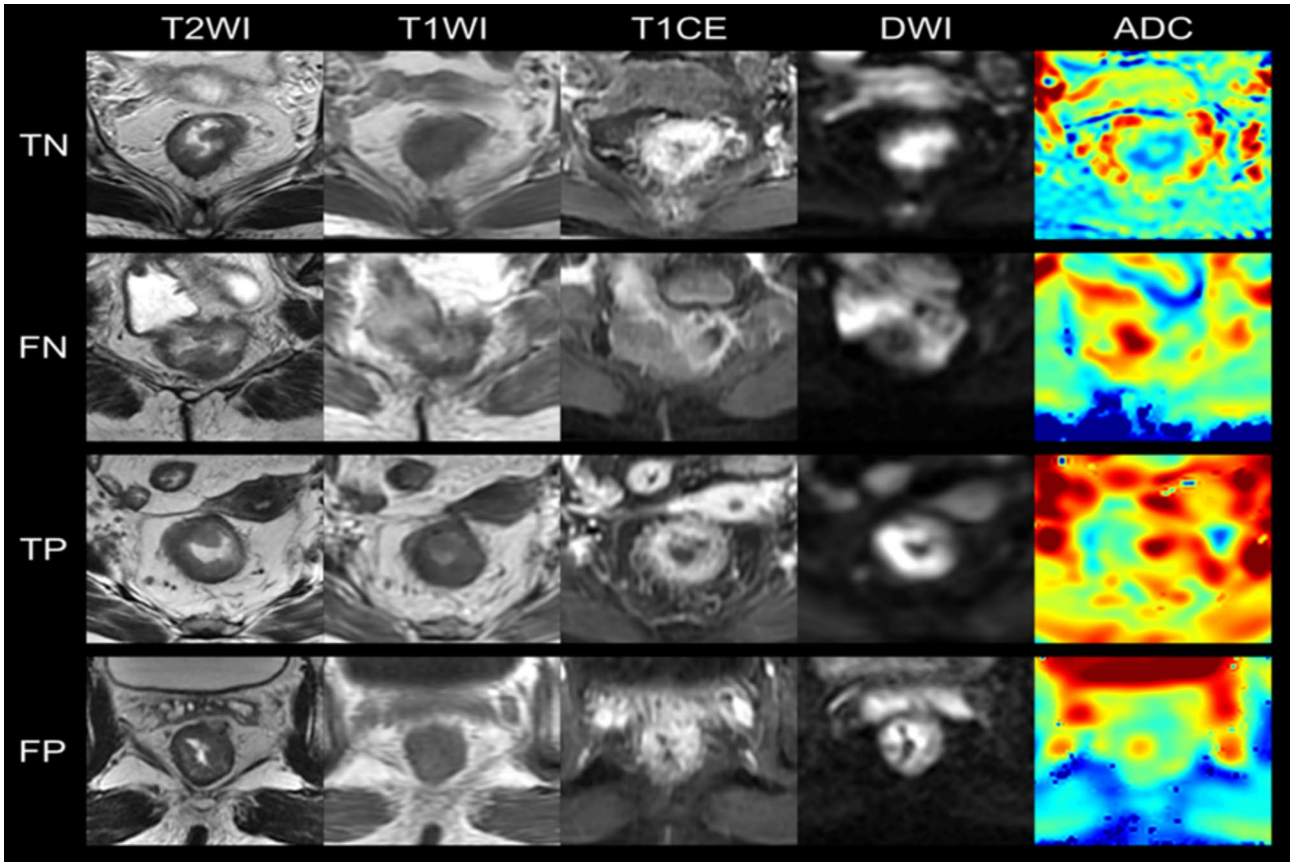

Fig. 2 Representative images of rectal cancer patients. T2WI (T2-weighted imaging), T1WI (T1-weighted imaging), T1CE (contrast-enhanced T1WI), DWI (diffusion-weighted imaging), and ADC (apparent diffusion coefficient) images from 4 representative patients in the validation dataset, indicating the true negative, false negative, true positive, and false positive prediction by the Combined DL(deep learning) model

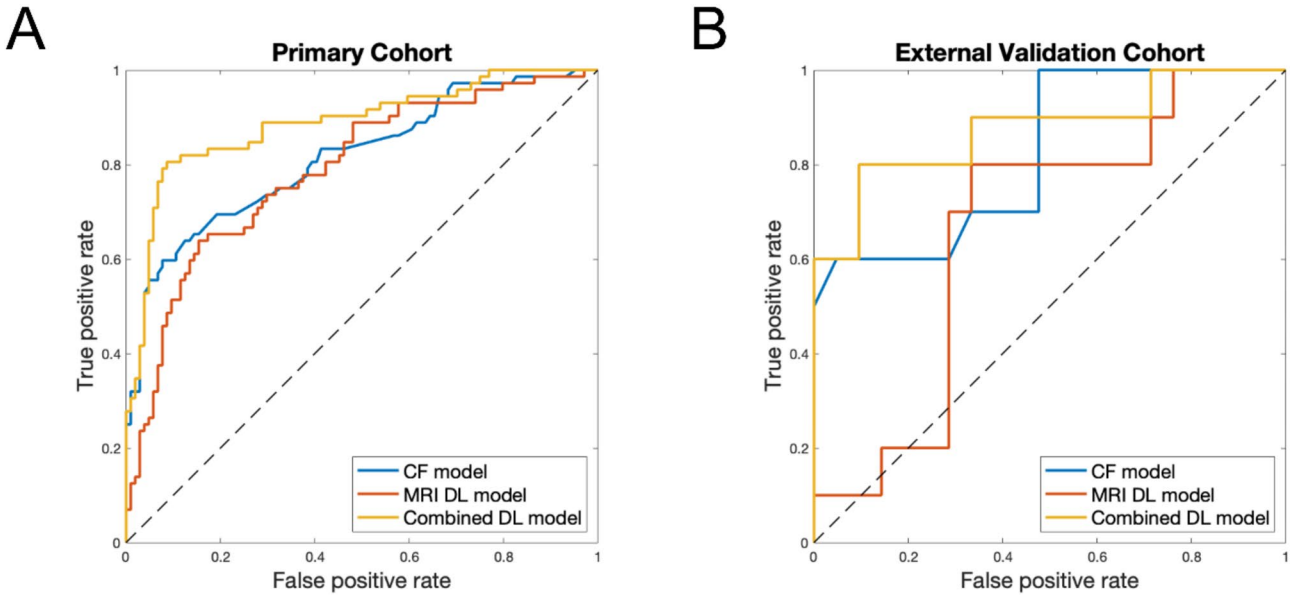

Fig. 3 Receiver operating characteristic curves in discriminating SLM (synchronous liver metastasis) and non-SLM from three models in the primary study cohort (**A**) and external validation cohort (**B**)

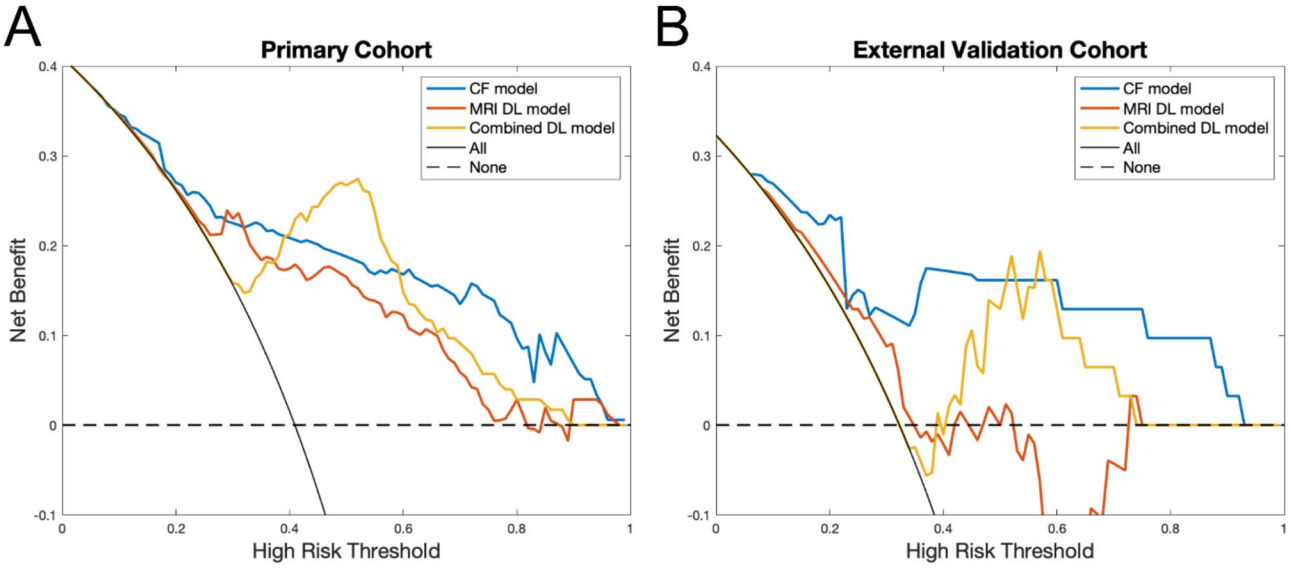

Fig. 4 Decision curve analysis of the three models in the primary study cohort (**A**) and external validation cohort (**B**)

patients), 50.0% (5/10 patients), 100% (21/21 patients), 100% (5/5 patients), and 80.8% (21/26 patients), respectively. For the MRI DL model, the ACC, SEN, SPE, PPV, and NPV were 67.7% (21/31 patients), 80.0% (8/10 patients), 61.9% (13/21 patients), 50.0% (8/16 patients), and 86.7% (13/15 patients), respectively. For the Combined DL model, the ACC, SEN, SPE, PPV, and NPV were 80.6% (25/31 patients), 80.0% (8/10 patients), 81.0% (17/21 patients), 66.7% (8/12 patients), and 89.5% (17/19 patients), respectively. ROC curves in discriminating non-SLM and SLM groups from three models in the external validation cohort are illustrated in Fig. 3B.

The clinical benefit was confirmed by decision curve analysis, Fig. 4A and B.

Discussion

Early diagnosis of atypical hepatic lesions in patients with RC remains a challenge. In this two-center study, we explored the value of the DL approach in identifying patients at high risk for SLM based on basic clinical data and pre-treatment multiparametric MRI of primary lesions, using only routinely examination data. Clinical factors such as sex, primary tumor site, CEA level, and CA19-9 level were included. MRI sequences including T1WI, T2WI, T1CE, DWI, and ADC images were applied. We demonstrated that DL models displayed powerful predictive ability in predicting high/low-risk stratification of patients for SLM. Combining DL features extracted from multiparametric MRI with clinical factors achieved better predictive performance compared to DL features or clinical factors only. Furthermore, these models exhibited stability, which validated in the external cohort. According to the DL models, the presence of liver metastases should be strongly suspected when cases in which the risk probability of metastases calculated by the combined model of atypical liver lesions is high. In such high-risk cases, a more aggressive systemic examination and shorter follow-up should be considered. The clinical benefit was confirmed by decision curve analysis.

Tumor markers CEA and CA19-9 are widely recognized as crucial factors in the diagnosis, treatment decision, and prognosis. Previous studies have revealed that laboratory examinations such as CEA and CA199 can predict synchronous distant metastasis in patients with RC [21–23], which aligns with our findings. Some researchers have estimated the risk of metastasis using clinicopathological variables such as pathological grade and T stage, and found that these variables also contributed to metastasis risk stratification [23, 24]. However, certain pathological features can only be obtained surgically and are rooted in the subjective nature of the evaluation process. The indicators used in clinical practice should be as simple, objective and non-invasive as possible. Therefore, in our study, we specifically selected clinical factors, including sex, primary tumor site, CEA level, and CA19-9 level, to establish the CF model. These indicators can be readily obtained from routine pretreatment examinations.

Radiomics has emerged as a noninvasive and efficient method for quantitatively describing tumor heterogeneity [25]. Previous studies found that radiomic features extracted from primary RC lesions can stratify the risk of synchronous metastases, providing guidance for staging and treatment decisions [14, 15, 26]. While MRI radiomics analysis has shown promising predictive value for rectal cancer with distant metastases, these studies adopted only single type of MRI image, neglecting the potential additional information that can be obtained

from multi-contrast images provided by various MRI sequences. Moreover, radiomics necessitates meticulous lesion delineation and the extraction and selection of hard-coded radiomic features [27]. DL approach allows for more flexible, effective, and accurate mapping between medical images and clinical outcomes by automatically learning relevant information through back-propagating adjustment of network parameters [28]. DL has the potential to reveal occult lesions that are hindered by current imaging methods, and different types of medical images can reflect diverse perspectives on pathological information [29, 30]. The study conducted by Liu et al. suggests that MRI-based DL radiomics exhibits potential in the prediction of distant metastases among RC patients undergoing neoadjuvant chemoradiotherapy (nCRT) and could assist in assessing the risk of distant metastases in patients with diverse responses to nCRT, achieving an AUC of 0.894 in the validation cohort [31]. The results of the study are promising. Hence, we proposed a DL approach based on multiparametric MRI images of primary lesions in RC. Additionally, we employed a relatively large patch image centered around the lesion as the input for DL, thereby including the surrounding regions of the tumor in the analysis and capturing the impact of microenvironmental data on metastases. The results demonstrated the utility of our proposed models in quantifying the risk of metastases in patients with uncertain hepatic nodules, thereby avoiding unnecessary delays in treatment. Patients with less than 1% risk for SLM may have the opportunity to receive individualized imaging test strategy, which may help decrease the costs associated with diagnostic evaluations and radiation exposure. Our DL approach can serve as an alternative method to improve the timeliness and accuracy of liver metastases detection, offering a valuable supplement to existing techniques.

This study had certain limitations that warrant discussion. Firstly, it was a retrospective analysis based on a relatively small sample size, which may limit the generalizability of the findings. The diminished advantage of the Combined DL model in the external cohort may reflect both the limited sample size. Small validation cohorts increase the risk of overestimating or underestimating model generalizability due to sampling bias. Future multi-center studies with larger, prospectively enrolled cohorts are needed to validate the clinical utility of the model across diverse populations and lesion characteristics. Secondly, the inclusion of small-sized metastases is insufficient. Reducing false negative results in the detection of small-sized SLM during preoperative examination remains a considerable challenge. To improving the treatment decision-making and decrease the costs associated with diagnostic evaluations, future studies should focus on investigating the application of DL models in predicting small metastases. Additionally, A limitation of this study is the selection of only the central 5 slices, which may overlook peripheral tumor heterogeneity. While a 3D volumetric approach may provide additional information, future research could further compare this approach to assess its potential benefits. Moreover, our study is the lack of advanced interpretability analysis, such as SHAP, to assess the contribution of clinical features and imaging data to model predictions. While we focused on model performance, future work will explore these techniques to provide clearer insights into their synergy. Lastly, as we chose a relatively shallow neural network to prevent overfitting in the training process, relevant information in the image may not be well learned. Therefore, further studies with an optimized DL framework should be conducted to improve the model performance and generalizability.

Conclusion

In conclusion, we successfully developed a DL model based on multiparametric MRI and clinical features to predict SLM in patients with RC. The model demonstrated satisfactory results and was validated in an external cohort. These findings highlighted the interplay between clinical and radiological findings to facilitate early and accurate diagnosis of SLM, leading to improved treatment options.

Abbreviations

SLM	Synchronous liver metastases
RC	Rectal cancer
DL	Deep learning
CF	Clinical feature
ROC	Receiver operating characteristic
AUC	Area under the curve
ACC	Accuracy
SEN	Sensitivity
SPE	Specificity
PPV	Positive predictive value

Supplementary Information

The online version contains supplementary material available at https://doi.org/10.1186/s12880-025-01692-3.

Supplementary Material 1

Acknowledgements

We thank all members of the author group for their efforts. We are also grateful for the support of all the patients and their families who participated in this work.

Author contributions

Jing Sun, Pu-Yeh Wu, and Dechun Zheng contributed to the methodology, study design, manuscript drafting, and critical revision of the manuscript for important intellectual content. Fangmin Shen, Xingfa Chen, Jieqiong She, Mingcong Luo, and Feifei Feng were responsible for data acquisition, analysis, and interpretation. All authors ensured the integrity of the entire study and approved the final manuscript.

Funding
This study has received funding from the Fujian Cancer Hospital Foundation (Grant No. YJ-YJ-05) and the Fujian Clinical Research Center for Radiation and Therapy of Digestive, Respiratory and Genitourinary Malignancies (Grant No. 2021Y2014).The funder had no role in the design of the study and collection, analysis, and interpretation of data or in writing the manuscript.

Data availability
The datasets used during the current study are available from the corresponding author on reasonable request.

Declarations

Ethical approval
The research protocol was approved by the Clinical Oncology School of Fujian Medical University and Fujian Medical University Union Hospital Ethics Committee (approval numbers: K2022-196-01 and 2023KY117). Given the retrospective nature of this study, the requirement for informed consent was waived. All methods were carried out in accordance with relevant guidelines and regulations. Our study adhered to the principles of the Declaration of Helsinki.

Consent for publication
The authors affirm that the human research participants provided informed consent for the publication of all images in the figures.

Competing interests
The authors declare no competing interests.

Author details
[1]Department of Radiology, Clinical Oncology School of Fujian Medical University, Fujian Cancer Hospital, No. 420, Fuma Road, Jin'an District, Fuzhou, Fujian 350014, China
[2]GE Healthcare, Beijing, China
[3]Department of Radiation Oncology, Fujian Medical University Union Hospital, Fuzhou, Fujian, China
[4]Department of Radiology, Fujian Medical University Union Hospital, Fuzhou, Fujian, China

Received: 13 April 2024 / Accepted: 25 April 2025
Published online: 19 May 2025

References

1. Siegel RL, Miller KD, Jemal A. Cancer statistics, 2019. Cancer J Clin. 2019;69(1):7–34.
2. Keller DS, Berho M, Perez RO, Wexner SD, Chand M. The multidisciplinary management of rectal cancer. Nat Rev Gastroenterol Hepatol. 2020;17(7):414–29.
3. Chow FC, Chok KS. Colorectal liver metastases: an update on multidisciplinary approach. World J Hepatol. 2019;11(2):150–72.
4. Chen X, Hu W, Huang C, Liang W, Zhang J, Wu D, et al. Survival outcome of palliative primary tumor resection for colorectal cancer patients with synchronous liver and/or lung metastases: A retrospective cohort study in the SEER database by propensity score matching analysis. Int J Surg. 2020;80:135–52.
5. Zhenghong ZZ, Guoweijian, Zhangning, Caiyunyun Y, et al. Retrospective study of predictors of bone metastasis in colorectal cancer patients. J Bone Oncol. 2017;9:25–8.
6. Gerlinger M, Rowan AJ, Horswell S, Math M, Larkin J, Endesfelder D, et al. Intratumor heterogeneity and branched evolution revealed by multiregion sequencing. N Engl J Med. 2012;366(10):883–92.
7. Schmidt VF, Öcal O, Walther V, Fabritius MP, Dietrich O, Kazmierczak PM, et al. Clinical benefits of MRI-guided freehand biopsy of small focal liver lesions in comparison to CT guidance. Eur Radiol. 2024.
8. Choi SH, Kim SY, Park SH, Kim KW, Lee JY, Lee SS, et al. Diagnostic performance of CT, gadoxetate disodium-enhanced MRI, and PET/CT for the diagnosis of colorectal liver metastasis: systematic review and meta-analysis. J Magn Reson Imaging: JMRI. 2018;47(5):1237–50.
9. Granata V, Fusco R, Catalano O, Avallone A, Palaia R, Botti G, et al. Diagnostic accuracy of magnetic resonance, computed tomography and contrast enhanced ultrasound in radiological multimodality assessment of peribiliary liver metastases. PLoS ONE. 2017;12(6):e0179951.
10. Rappeport ED, Loft A, Berthelsen AK, von der Recke P, Larsen PN, Mogensen AM, et al. Contrast-enhanced FDG-PET/CT vs. SPIO-enhanced MRI vs. FDG-PET vs. CT in patients with liver metastases from colorectal cancer: a prospective study with intraoperative confirmation. Acta Radiol (Stockholm Sweden: 1987). 2007;48(4):369–78.
11. Granata V, Fusco R, de Lutio di Castelguidone E, Avallone A, Palaia R, Delrio P, et al. Diagnostic performance of Gadoxetic acid-enhanced liver MRI versus multidetector CT in the assessment of colorectal liver metastases compared to hepatic resection. BMC Gastroenterol. 2019;19(1):129.
12. Lee JM, Yoon JH, Kim KW. Diagnosis of hepatocellular carcinoma: newer radiological tools. Semin Oncol. 2012;39(4):399–409.
13. Limkin EJ, Sun R, Dercle L, Zacharaki EI, Robert C, Reuzé S, et al. Promises and challenges for the implementation of computational medical imaging (radiomics) in oncology. Ann Oncol. 2017;28(6):1191–206.
14. Liu H, Zhang C, Wang L, Luo R, Li J, Zheng H, et al. MRI radiomics analysis for predicting preoperative synchronous distant metastasis in patients with rectal cancer. Eur Radiol. 2019;29(8):4418–26.
15. Liu M, Ma X, Shen F, Xia Y, Jia Y, Lu J. MRI-based radiomics nomogram to predict synchronous liver metastasis in primary rectal cancer patients. Cancer Med. 2020;9(14):5155–63.
16. Zhu HB, Xu D, Ye M, Sun L, Zhang XY, Li XT, et al. Deep learning-assisted magnetic resonance imaging prediction of tumor response to chemotherapy in patients with colorectal liver metastases. Int J Cancer. 2021;148(7):1717–30.
17. Wei J, Cheng J, Gu D, Chai F, Hong N, Wang Y, et al. Deep learning-based radiomics predicts response to chemotherapy in colorectal liver metastases. Med Phys. 2021;48(1):513–22.
18. He K, Zhang X, Ren S, Sun J. Deep Residual Learning for Image Recognition. 2016 IEEE Conference on Computer Vision and Pattern Recognition (CVPR). 2016:770-8.
19. Rimm DL, Leung SCY, McShane LM, Bai Y, Bane AL, Bartlett JMS, et al. An international multicenter study to evaluate reproducibility of automated scoring for assessment of Ki67 in breast cancer. Mod Pathology: Official J United States Can Acad Pathol Inc. 2019;32(1):59–69.
20. Huang JX, Yan W, Song ZX, Qian RY, Chen P, Salminen E, et al. Relationship between proliferative activity of cancer cells and clinicopathological factors in patients with esophageal squamous cell carcinoma. World J Gastroenterol. 2005;11(19):2956–9.
21. Ding X, Sun D, Guo Q, Li Y, Chen H, Dai X, et al. The value of diffusion kurtosis imaging and intravoxel incoherent motion quantitative parameters in predicting synchronous distant metastasis of rectal cancer. BMC Cancer. 2022;22(1):920.
22. Yan Y, Liu H, Mao K, Zhang M, Zhou Q, Yu W, et al. Novel nomograms to predict lymph node metastasis and liver metastasis in patients with early colon carcinoma. J Transl Med. 2019;17(1):193.
23. Gaitanidis A, Alevizakos M, Tsaroucha A, Tsalikidis C, Pitiakoudis M. Predictive nomograms for synchronous distant metastasis in rectal Cancer. J Gastrointest Surg. 2018;22(7):1268–76.
24. Gaitanidis A, Machairas N, Alevizakos M, Tsalikidis C, Tsaroucha A, Pitiakoudis M. Predictive nomograms for synchronous liver and lung metastasis in Colon cancer. J Gastrointest Cancer. 2020;51(3):925–31.
25. Ren S, Zhao R, Zhang J, Guo K, Gu X, Duan S, et al. Diagnostic accuracy of unenhanced CT texture analysis to differentiate mass-forming pancreatitis from pancreatic ductal adenocarcinoma. Abdom Radiol (New York). 2020;45(5):1524–33.
26. Shu Z, Fang S, Ding Z, Mao D, Cai R, Chen Y, et al. MRI-based radiomics nomogram to detect primary rectal cancer with synchronous liver metastases. Sci Rep. 2019;9(1):3374.
27. Zheng X, Yao Z, Huang Y, Yu Y, Wang Y, Liu Y, et al. Deep learning radiomics can predict axillary lymph node status in early-stage breast cancer. Nat Commun. 2020;11(1):1236.
28. Mazurowski MA, Buda M, Saha A, Bashir MR. Deep learning in radiology: an overview of the concepts and a survey of the state of the Art with focus on MRI. J Magn Reson Imaging: JMRI. 2019;49(4):939–54.
29. Kuntz S, Krieghoff-Henning E, Kather JN, Jutzi T, Höhn J, Kiehl L, et al. Gastrointestinal cancer classification and prognostication from histology using deep learning: Systematic review. European journal of cancer (Oxford, England: 1990). 2021;155:200–15.
30. Avanzo M, Wei L, Stancanello J, Vallières M, Rao A, Morin O, et al. Machine and deep learning methods for radiomics. Med Phys. 2020;47(5):e185–202.

31. Liu X, Zhang D, Liu Z, Li Z, Xie P, Sun K, et al. Deep learning radiomics-based prediction of distant metastasis in patients with locally advanced rectal cancer after neoadjuvant chemoradiotherapy: A multicentre study. EBioMedicine. 2021;69:103442.

Publisher's note